Available Online: 19 November 2026 DOI: 10.54254/3029-0880/2026.39054

Constrained route optimization on the Brenta mountain trail network

***Jiaxuan Wu*[1,*], *Haozhuo Bo*[2], *Chongyuan Xu*[3], *Xiyu Meng*[4]**

[1]WLSA Shanghai Academy, Shanghai, China
[2]Qingdao Academy, Qingdao, China
[3]Qihua Academy, Nanchang, China
[4]Shanghai United International School Hefei Campus, Hefei, China

*Corresponding Author. Email: xdpan19820627@gmail.com

Abstract. Routing over mountainous terrain is a challenging problem, as a practical route has to consider the horizontal distance as well as the extra cost incurred by elevation changes. This study investigates preference - based route optimization within a Digital Elevation Model (DEM)-integrated mountain trail network in the Brenta Dolomites, Trentino, northern Italy. A Digital Elevation Model (DEM) is a way of modeling terrain on a computer, taking a continuous landscape and turning it into a grid of discrete, connected points with different movement costs. Previous studies have shown that DEM-based least-cost path techniques and the Dijkstra's algorithm can effectively search for pathways in mountainous terrains. These methods, however, are typically based on a predefined cost function and have limited capability to incorporate explicit terrain constraints. For spatial planning problems, mathematical optimization methods have been applied to handle complex constraints and decision variables. This research extends these ideas by developing a constrained optimization framework for route selection in an integrated mountain trail system of a DEM. This study addresses that question by constructing a real, DEM-derived weighted graph for Brenta Dolomites, a mountain group in Trentino, northern Italy, near Madonna di Campiglio, in which nodes represent discrete terrain locations and edges represent feasible movements between neighboring cells. Each edge is assigned a cost that combines horizontal distance with a physically motivated penalty for elevation change, so that the resulting network reflects real physical effort rather than map distance. Dijkstra's algorithm is used as a way to find the shortest path. Mathematical optimization is used to add rules that can't be handled well by finding the shortest path. Comparing with ways to plan routes is also used to check the routes based on distance climbing how fast they run on a computer and if they follow the rules. The results show that adding rules about the land can make a choice between how the path is and how much climbing is needed. The study gives a way to see when extra rules make the path change and how better path planning can match wishes of people, in mountain areas.

Keywords: mountain trail networks, resource-constrained shortest path, mixed-integer programming, digital elevation model, Dijkstra algorithm

Copyright: © 2026 by the authors. Submitted for possible open access publication under the terms and conditions of the Creative Commons Attribution (CC BY) license (https://creativecommons.org/licenses/by/4.0/).

1. Introduction

Mountain trails form complex transportation networks, and choosing a route on them is affected by more than geographical distance. In relatively flat environments, the shortest path between two locations may provide the best route. In mountainous terrain, however, differences in elevation, slope and terrain conditions can substantially affect the effort and time required to travel between two points. Consequently, a route that minimizes distance may not necessarily be the most appropriate route for a particular hiker. This creates a route optimization problem.

Geographical Information Systems (GIS) and network optimization provide established approaches for representing and analyzing such problems. A physical trail network can be represented as a weighted graph. In that graph, locations are represented by nodes and trail segments by edges or directed arcs. Attributes derived from spatial data can then be assigned to each arc and incorporated into an optimization model. This approach allows real-world terrain characteristics to be transformed into mathematical parameters that can be used to compare routes.

Previous research has demonstrated the applicability of optimization methods to forest and mountainous route planning. Gumus and Turk [1] developed a skid-trail pattern using Linear Programming (LP) together with GIS. Their study demonstrated how an LP model could be combined with spatial information to improve the design of forest transportation routes and reduce operational and environmental impacts. This illustrates the potential of mathematical programming to incorporate multiple constraints into spatial route planning.

Graph-based shortest-path methods have also been widely applied to forest and mountainous networks. Parsakhoo and Jajouzadeh [2] applied Dijkstra's algorithm to forest road planning, representing the network using nodes and links and assigning costs according to factors including link length, longitudinal gradient and side slope. Their results showed that Dijkstra's algorithm could find an optimal path according to construction cost. This provides a useful basis for using Dijkstra's algorithm as a baseline approach in mountain route optimization.

Rees [3] specifically investigated least-cost paths in mountainous terrain using a Digital Elevation Model (DEM). The study incorporated terrain-related costs into a least-cost path analysis and used Dijkstra's algorithm to identify routes through mountainous landscapes. The results highlighted the importance of terrain-dependent cost functions when evaluating routes in mountainous environments.

GIS-based decision-support systems provide another relevant direction. Sferlazza et al. [4] developed a GIS-based decision support system for forest accessibility in the Madonie Mountains in Sicily. Their framework integrated spatial analysis and least-cost path methods to support decisions concerning forest accessibility and resource management. This demonstrates how terrain-based network analysis can be incorporated into a broader decision-support framework.

These studies show how graph algorithms and mathematical programming can support terrainrelated route planning [1-4]. A shortest-path algorithm finds a minimum-cost route once additive arc costs are defined. However, in reality, additional requirements can change which routes are feasible, such as a cumulative ascent budget or an altitude-weighted exposure cap. A hiker seeking a short journey may therefore select a different route from one seeking less climbing. We examine these trade-offs on a fixed mountain trail network, asking when the added requirements change the optimal route and how much distance or estimated time they cost.

This study has two aims. The first is to construct a terrain-aware route-optimization framework for the Brenta Dolomites using GPX trail connections and DEM elevations, and to verify that the computed routes satisfy the stated models. The second is to examine how route selection changes when ascent, altitude-weighted exposure, and grade requirements are imposed. These requirements allow us to explore trade-offs between route characteristics.

2. Data and methods

2.1. Study area and network data

The study covers part of the Brenta Dolomites near Madonna di Campiglio in Trentino, northern Italy. We construct the directed graph $G = (V, A)$ from ten GPX tracks and assign elevations from the Copernicus GLO-30[1]. Embedded links associate eight tracks with Outdooractive and two with Trentino.com (Appendix A). All 13,202 original GPX points fall within the tile's approximate bounds of 10°–11°E and 46°–47°N. The tracks were resampled at 80 m intervals in projected coordinates. After that, spatial merging of the resampled points produced 810 network nodes. We connect two distinct nodes when they occur on at least one mapped track. This gives 832 physical edges. Allowing travel in both directions produces 1,664 directed arcs, whose ascent and time costs depend on direction. Table 1 summarizes the resulting network.

Table 1. Network construction summary

Stage	Count	Basis
GPX track files	10	8 Outdooractive; 2 Trentino.com
Merged nodes $\|V\|$	810	Spatial consolidation
Physical edges $\|E\|$	832	Consecutive mapped nodes
Directed arcs $\|A\|$	1,664	Two directions per physical edge

The two Origin–Destination (OD) pairs connect the following representative hut nodes.
OD1: Rifugio Tuckett (node 119, 2,267 m) → Rifugio Tosa Pedrotti (node 282, 2,487 m)
OD2: Rifugio Graffer (node 46, 2,262 m) → Rifugio Tosa Pedrotti (node 282, 2,487 m)

2.2. Arc cost specification

Let the directed network be $G = (V, A)$, with origin o and destination q. For arc (i, j), let $d_{ij} > 0$ denote horizontal distance in meters and z_i denote DEM elevation in meters. Positive gain g_{ij}, loss l_{ij}, and signed endpoint grade s_{ij} are defined by Equation (1).

$$g_{ij} = max(0,\ z_j - z_i), \quad l_{ij} = max(0,\ z_i - z_j), \quad s_{ij} = \frac{z_j - z_i}{d_{ij}} \tag{1}$$

Reversing an arc changes the sign of its elevation difference. The same segment has different ascent and travel-time costs in each direction.

We estimate a terrain-sensitive speed proxy that depends on slope based on Tobler's hiking function [5]. Equation (2) expresses speed in km/h and arc time in hours. Applying the same rule to every arc gives a consistent basis for comparing routes.

$$v_{ij} = max\{0.5,\ 6exp(-3.5|s_{ij} + 0.05|)\}, t_{ij} = \frac{d_{ij}}{1000\, v_{ij}} \tag{2}$$

Altitude-weighted exposure is calculated from mean endpoint elevation. The index rises linearly from zero at 2,200 m to one at 2,700 m and remains within [0, 1]. Multiplying this index by arc distance produces a weighted-distance contribution a_{ij} in kilometers:

[1] Copernicus Data Space Ecosystem. (n.d.). Global and European Digital Elevation Model. https://dataspace.copernicus.eu/explore-data/data-collections/copernicus-contributingmissions/collections-description/COP-DEM

$$h_{ij} = clip\{\frac{(z_i+z_j)/2-2200}{500}, 0, 1\}, a_{ij} = \frac{d_{ij}h_{ij}}{1000} \tag{3}$$

The 2,200 m and 2,700 m thresholds are assumptions of this study. A kilometer at an index of 0.5 contributes 0.5 weighted km.

2.3. Dijkstra baseline and computational scope

Dijkstra's algorithm [6] finds shortest paths when arc costs are nonnegative. We apply it to the same directed graph as the optimization models, using $w(u, v) = d_{uv}$ for the distance baseline. Other nonnegative additive weights can be used without changing the graph.

Let $L(v)$ denote the tentative cost from the origin to node v. Initialize $L(o) = 0$ and $L(v) = +\infty$ for all other nodes. At each iteration, select the unfinalized node u with the smallest finite label, finalize it, and relax each outgoing arc:

$$L(v) \leftarrow minL(v), L(u) + w(u, v). \tag{4}$$

When a label improves, we record u as the predecessor of v. The search ends when the destination is finalized or no reachable unfinalized node remains. In the first case, the predecessor sequence reconstructs the route; in the second, no route exists. With a binary-heap priority queue, the running-time bound is $O((|V| + |A|)log|V|)$.

Finalization is valid because extending a path with nonnegative costs cannot lower its accumulated cost. Both distance and estimated time satisfy this condition. A grade limit is also straightforward to handle by removing arcs that exceed it before search. Cumulative ascent and altitude-weighted exposure limits require more information: the cheapest label at a node may have used too much of the remaining resource budget. A single cost label per node is therefore insufficient in general [7], which motivates the explicit budgets in Models 2 and 3.

2.4. Optimization formulations

First, we use a basic network-flow formulation to identify the shortest path. Let x_{ij} indicate whether arc (i, j) is selected. The node–arc incidence matrix B assigns +1 at an arc's tail and −1 at its head. The demand vector b is +1 at o, −1 at q, and zero elsewhere. Model 1 minimizes total distance subject to single-unit flow conservation:

$$min\ d^T x \quad s.t. \quad Bx = b,\ 0 \le x \le 1 \tag{5}$$

The vectors d, g, t, and a contain the arc attributes defined above. Total unimodularity of the node– arc incidence matrix, together with integer demands and bounds, guarantees an integral optimal extreme point for Model 1. We can therefore solve it as an LP. The archived solutions are integral and match the minimum distance returned by Dijkstra's algorithm.

Flow conservation alone allows cycles. Here, every arc has strictly positive distance and time costs, while resource contributions are nonnegative. Removing a cycle preserves the required flow, uses no more resource, and lowers the objective. An optimal solution consequently has a simple-path representation. We also reconstruct the ordered route to check continuity and exclude disconnected selected components.

Model 2 minimizes distance with a cumulative ascent budget $\overline{G}$. Keeping the objective unchanged allows us to isolate the effect of this added requirement: it finds the route with the smallest distance among all routes whose total climbing stays below the chosen budget.

$$min\ d^T x \quad s.t. \quad Bx = b, \quad g^T x \le \overline{G}, \quad x \in \{0, 1\}^{|A|} \tag{6}$$

The ascent row removes the general integrality guarantee of the network LP, so we use binary variables to select a single route. If the distance-optimal route exceeds the budget, Model 2 may select a longer one. The extra distance then measures the cost of meeting the ascent requirement.

Model 3 minimizes estimated travel time while retaining the ascent budget and adding an altitude - weighted exposure cap H and an absolute-grade limit S. Define $u_{ij}(S) = 1$ when $|s_{ij}| \le S$ and zero otherwise. The complete model is:

$$min\ t^T x \quad s.t. \quad Bx = b, \quad g^T x \le \overline{G}, \quad a^T x \le H \tag{7}$$

$$0 \le x_{ij} \le u_{ij}(S) \quad for\ all\ (i,j) \in A, \quad x \in \{0,1\}^{|A|} \tag{8}$$

The grade limit applies to each arc separately: an arc is unavailable if its absolute grade exceeds S. Ascent and altitude-weighted exposure, by contrast, are summed over the route.

2.5. Altitude-weighted exposure constraint analysis

To characterize constraint activation, fix an OD pair, an ascent budget $\overline{G}$, and a grade limit $\overline{S}$. Let $P(\overline{G}, \overline{S})$ be the finite, nonempty set of simple routes satisfying those two requirements. Define T_0 as the fastest time over this set and E_{min} as its minimum altitude-weighted exposure. To account for possible ties among fastest routes, define E_{fast} as the smallest altitude-weighted exposure attained by any route with time T_0:

$$T_0 = t^T x, \quad E_{min} = a^T x \tag{9}$$

$$E_{fast} = min\{a^T x : x \in P,\ t^T x = T_0\} \tag{10}$$

For any altitude-weighted exposure cap H, the optimal value of Model 3 over this fixed route set is:

$$T^*(H) = min\{t^T x : x \in P,\ a^T x \le H\}, \quad min\emptyset = +\infty \tag{11}$$

Proposition 1. If $H < E_{min}$, no route is feasible. If $E_{min} \le H < E_{fast}$, at least one route is feasible but every feasible route is slower than T_0. If $H \ge E_{fast}$, at least one fastest route remains feasible and $T^*(H) = T_0$. The middle regime is empty when $E_{min} = E_{fast}$.

Proof. Below E_{min}, the definition of the minimum altitude-weighted exposure excludes every route. At or above E_{min}, an altitude-weighted exposure-minimizing route is feasible. Below E_{fast}, no route attaining T_0 satisfies the altitude-weighted exposure cap, so finiteness of P implies a strictly larger optimal time. At or above E_{fast}, a route attaining both T_0 and an admissible altitude-weighted exposure exists; restricting P cannot yield a value below T_0. These observations establish all three statements.

Relaxing H enlarges the feasible set, so $T^*(H)$ cannot increase. Since only finitely many routes are available, changes occur in steps. Tightening the cap may leave the optimum unchanged, force a slower route, or remove every feasible route. For a feasible cap, we report the additional time as:

$$\Delta T(H) = T^*(H) - T_0 \ge 0. \tag{12}$$

We evaluate altitude-weighted exposure tightening through these discrete changes rather than assign it a continuous shadow price. A positive $\Delta T(H)$ is the time cost of meeting the cap. Its interpretation depends on whether the associated altitude-weighted exposure reduction matters to the user.

3. Experimental design

3.1. Parameter specification

The original ascent cap is the midpoint between Model 1 ascent and a minimum-ascent reference. Altitude-weighted exposure uses the midpoint between Model 1 altitude-weighted exposure and an unrestricted minimum-altitude-weighted exposure reference, raised if necessary to keep Model 2 feasible. The grade limit equals the maximum absolute grade on the Model 2 route:

$$\overline{G} = \frac{\overline{G}_1+\overline{G}_{min}}{2}, \quad H = max\{\frac{E_1+E_{ref}}{2}, E_2\}, \quad S = S_2. \tag{13}$$

Subscripts 1 and 2 in Equation (13) identify the selected routes from Models 1 and 2. E_{ref} is the minimum-altitude-weighted exposure reference computed without the later ascent and grade restrictions. It differs from the constrained minimum used in Section 4.3. Table 2 lists the original constraint settings for both OD pairs.

Table 2. Original constraint settings. Altitude-weighted exposure is in weighted km; grade is dimensionless

Case	Ascent cap $\overline{G}$ (m)	Altitude-weighted exposure cap $\overline{H}$	Grade cap $\overline{S}$
OD1	731.972	1.936714	0.769317
OD2	1,025.445	2.911748	0.769317

These limits depend on the routes being compared. In particular, the altitude-weighted exposure and grade limits keep the Model 2 route feasible by construction. They are useful for examining model behavior. Whether that feasible route is also the fastest is a separate question, tested by the time-only variant.

3.2. Evaluation protocol

We compare the three models using distance, ascent, estimated time, altitude-weighted exposure, and maximum absolute grade. We then solve five variants with the same time objective: time only; time with ascent; time with ascent and altitude-weighted exposure; time with ascent and grade; and the full formulation. Holding the objective fixed makes it possible to attribute any change to the added constraints.

To measure the remaining improvement opportunity, we minimize altitude-weighted exposure with the original ascent and grade limits fixed. Denote the resulting value by E_{min} and the altitude-weighted exposure of the original time-optimal route by E_0. The maximum possible percentage reduction is $100(E_0 - E_{min})/E_0$. Four scenarios impose $H(r) = (1 - r)E_0$ for r = 0, 0.0001, 0.001, and 0.01, corresponding to reduction requirements of 0%, 0.01%, 0.1%, and 1%. Each feasible scenario then minimizes time. The altitude-weighted exposure rows are scaled to weighted meters during these solves to improve numerical conditioning; reported results remain in weighted kilometers.

We inspect LP relaxations to see whether fractional solutions arise. For runtime, we report the median of 15 solve-only repetitions for each method and OD pair. Input loading, graph construction, calibration, and export are excluded.

The implementation uses SciPy's LP and mixed-integer programming interfaces with HiGHS[2]. The extended analysis requests a zero relative MIP gap and allows 120 s per solve. We check graph dimensions,

[2] SciPy Developers. (n.d.). scipy.optimize.milp. SciPy reference manual. https://docs.scipy.org/doc/scipy/reference/generated/scipy.optimize.milp.html

arc identities, flow balance, route continuity, and resource compliance. Then compare the exported arc sums with the reported route metrics. Recalculating the coefficients also checks Equations (1)–(3), including the speed floor. Fourteen additional solves reproduce the principal objectives and both definitions of the altitude-weighted exposure reference, with solver-reported zero MIP gaps.

These checks establish that the reported routes solve the stated problems on the archived inputs. Observed journey times and an external measure of altitude-weighted exposure are unavailable, so predictive accuracy remains untested.

4. Results

4.1. Route characteristics

Figure 1 compares the selected routes on the complete study network. Table 3 reports their distance, ascent, estimated time, and altitude-weighted exposure under the original constraint settings.

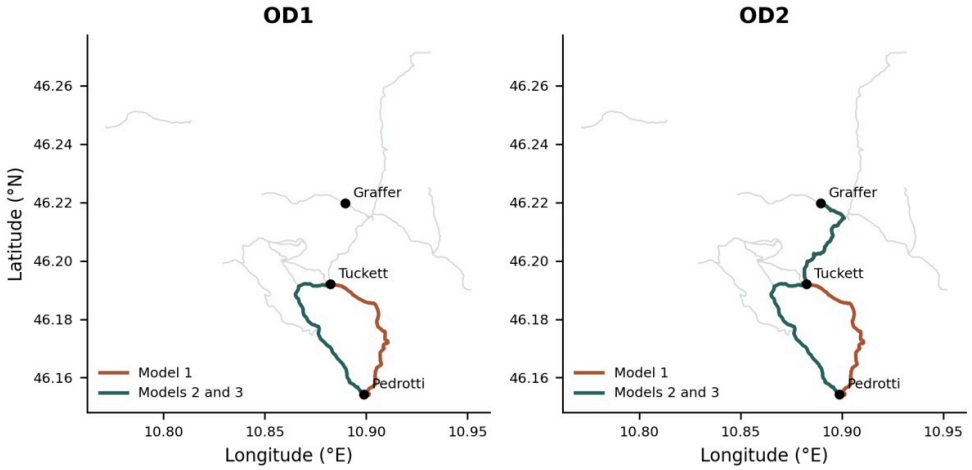


Figure 1. Model routes on the GPX-derived network. Gray lines show all 832 physical edges. Model 1 is the distance optimum; Models 2 and 3 coincide under the original parameter settings. Coordinates are geographic, and plotted node positions come from the master network table

Table 3. Main model results under the original constraints. Time is estimated walking time

Case and model	Distance (km)	Ascent (m)	Time (min)	Exposure (w. km)
OD1 M1	6.353	814.16	178.78	3.102482
OD1 M2	6.611	649.78	143.05	0.787330
OD1 M3	6.611	649.78	143.05	0.787330
OD2 M1	10.925	1,107.63	255.02	4.077516
OD2 M2	11.183	943.26	219.29	1.762364
OD2 M3	11.183	943.26	219.29	1.762364

The ascent budget changes the selected corridor in both OD cases. For OD1, distance rises from 6.353 to 6.611 km (4.06%), while ascent falls by 20.19%. For OD2, the corresponding changes are +2.36% and

−14.84%. Both routes gain 258.15 m in length and lose 164.38 m in ascent because they use the same replacement corridor. The two cases therefore illustrate the same network mechanism.

The longer routes also have shorter estimated times: 143.05 instead of 178.78 min for OD1, and 219.29 instead of 255.02 min for OD2. These reductions, about 19.99% and 14.01%, follow from evaluating all routes with the same terrain-dependent time coefficients. Model 2 minimizes distance under an ascent limit. Figure 2 shows the lower-elevation corridor that produces this result.

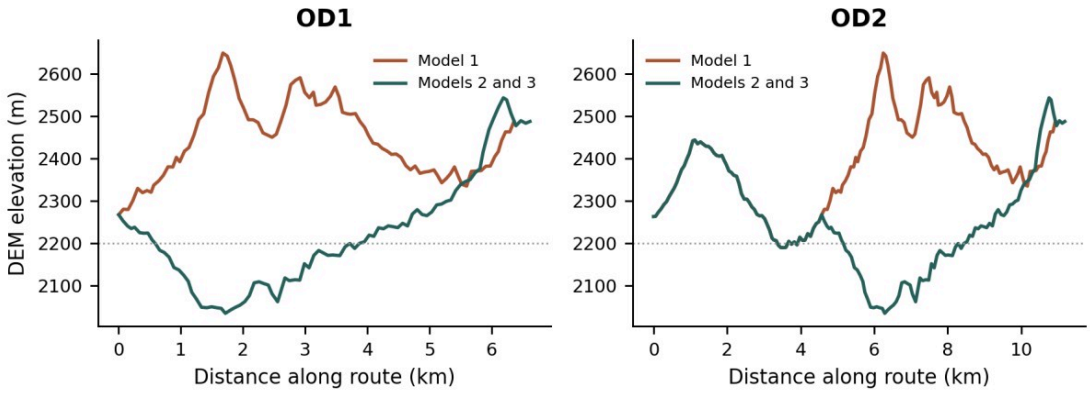


Figure 2. Elevation profiles of the selected routes. The dotted line marks the 2,200 m lower threshold of the altitude-weighted exposure index. Profiles are plotted against each route's own cumulative distance; corresponding horizontal positions do not necessarily denote the same location

The ascent reduction comes with a higher maximum endpoint grade. In both cases, the largest absolute grade rises from 0.72 in Model 1 to 0.77 in Models 2 and 3. Thus, a route with less total climbing is not necessarily gentler at its steepest edge. The original Model 3 grade limit permits the steepest edge of the Model 2 route.

4.2. Constraint ablation and integrality

Table 4 summarizes controlled ablation results. Under the original parameter settings, all five time-objective variants select the same arc set within each OD pair, with estimated times of 143.05 min and 219.29 min. The time-only solution already satisfies all three original limits. Adding those limits leaves that optimum available and cannot produce a faster solution. Therefore, Model 3 leaves the route unchanged at these internally calibrated settings. However, if we have tighter requirements, there may be some effect.

Table 4. Controlled ablation with the time objective held fixed. "Same" means identical selected arc sets within each OD

Constraint blocks	OD1 time (min)	OD2 time (min)	Route outcome
None	143.04645	219.28779	Same
Ascent	143.04645	219.28779	Same
Ascent and altitude-weighted exposure	143.04645	219.28779	Same
Ascent and grade	143.04645	219.28779	Same
Ascent, altitude-weighted exposure, grade	143.04645	219.28779	Same

This result requires a distinction between a tight constraint and a constraint that changes the solution. The ascent and altitude-weighted exposure budgets have slack of 82.19 m and 1.15 weighted km, respectively, in both cases. The grade limit is attained exactly, yet removing it does not change the optimum.

The Model 2 LP relaxation selects 176 fractional arcs in each case. Its objective lies 1.95% below the integer optimum for OD1 and 1.15% below it for OD2, using the integer objective as the denominator. Such fractional arc selections do not describe a single hiking route, which confirms the need to retain integrality. Model 3 has an integral LP optimum under the original caps in these instances.

4.3. Altitude-weighted exposure sensitivity

With the original ascent and grade limits fixed, minimizing altitude-weighted exposure leaves very little room for improvement (Table 5).

Table 5. Exposure improvement available under the fixed original ascent and grade limits

Quantity	OD1	OD2
Original route E_0 (weighted m)	787.329916	1,762.363925
Minimum Emin (weighted m)	787.136703	1,762.170713
Maximum reduction (weighted m)	0.193212	0.193212
Maximum reduction (%)	0.02454	0.01096

The unrestricted altitude-weighted exposure references, 770.95 and 1,745.98 weighted m, are lower than these constrained minima. They were computed over a larger set of routes for parameter calibration. Using them as the attainable altitude-weighted exposure floor under the original ascent and grade limits would overstate the available improvement.

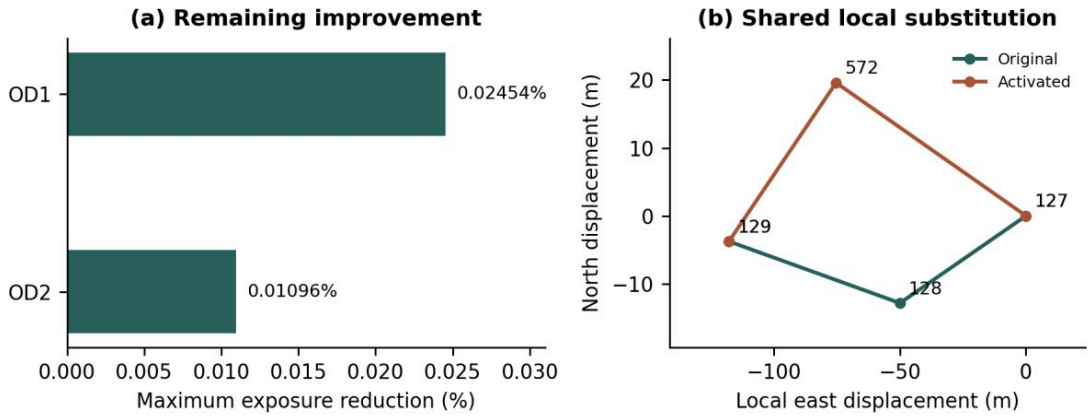


Figure 3. Remaining altitude-weighted exposure improvement and its spatial mechanism. Panel (a) reports the maximum percentage reduction under fixed ascent and grade limits. Panel (b) shows the shared local detour using approximate displacements derived from node coordinates. Weighted exposure reduction is not equivalent to physical distance saved

Requiring a 0.01% altitude-weighted exposure reduction selects the minimum-altitude-weighted exposure alternative for both OD pairs. It adds 6.25 m and an estimated 2.06 s, with no change in ascent. Both routes replace 127 → 128 → 129 with 127 → 572 → 129. This shared two-arc detour accounts for the identical

absolute differences shown in Figure 3. Table 6 summarizes the outcomes under the stricter exposure requirements.

Table 6. Stricter exposure requirements relative to E_0. The 0% row uses $H = E_0$, already tighter than the original cap H

Required reduction	OD1 time (min)	OD2 time (min)	Outcome
0%	143.04645	219.28779	Original route
0.01%	143.08071	219.32206	Local detour
0.1%	—	—	Infeasible
1%	—	—	Infeasible

Requirements of 0.1% and 1% are infeasible because their altitude-weighted exposure caps lie below Emin. The minimum-altitude-weighted exposure solve establishes this limit for the fixed ascent and grade constraints. The feasible 0.01% reduction, however, is too small to support a claim of practical improvement without testing uncertainty in the elevations, graph construction, and time coefficients.

4.4. Baseline agreement and computational performance

Dijkstra's algorithm and Model 1 return the same minimum distance for both OD pairs, providing a check through two different solution methods. The route changes in Section 4.1 arise when the objective or constraints change. They are not evidence that one solver finds a better answer to the same optimization problem.

Table 7 reports the median solve times from 15 repetitions. Every method solves these instances quickly. Dijkstra and Model 1 address the same distance problem; Models 2 and 3 include additional requirements. Their runtimes therefore describe the computational cost of the formulations rather than rank interchangeable algorithms.

Table 7. Archived median solve time over 15 repetitions. Values are in milliseconds; input preparation and export are excluded

Method	OD1 (ms)	OD2 (ms)
Dijkstra distance baseline	0.265	0.331
Model 1 LP	7.812	12.022
Model 2 MILP	11.808	42.057
Model 3 original MILP	10.128	11.223

The archived environment used Python 3.12.14, NumPy 2.3.5, pandas 2.2.3, and SciPy 1.17.0 on Linux x86-64.

5. Discussion

5.1. Interpretation

The comparison in Section 4.1 shows why distance alone is insufficient for evaluating these routes. Adding the ascent budget in Model 2 selects a corridor that is 258.15 m longer but requires 164.38 m less climbing. The relative changes differ between the two OD pairs because their total route lengths and ascent differ. However,

both use the same replacement corridor, so the agreement between them reflects a shared network feature rather than independent evidence that the same trade-off would occur elsewhere.

The lower-ascent routes also have shorter estimated travel times under the common speed function. This was not an objective of Model 2, which still minimizes distance subject to the ascent budget. The time reduction is a consequence of the route selected, and it illustrates how a modest increase in distance can be offset by a different elevation profile. Whether the predicted saving occurs in practice would need to be checked against observed walking times.

Model 3 retains the Model 2 route under the original settings. The parameter choices in Section 3.1 partly explain this result: the exposure and grade limits were chosen to keep that route feasible. The ablation in Section 4.2 establishes the other part of the explanation, showing that the route is already optimal for the time objective. Adding constraints that it satisfies cannot improve the minimum time or force a change of route. The grade limit is attained exactly, but removing it still leaves the optimum unchanged; a tight constraint need not affect the selected solution.

The exposure analysis in Section 4.3 then asks how much improvement remains within the fixed ascent and grade limits. The maximum reductions are only 0.02454% for OD1 and 0.01096% for OD2. A 0.01% requirement selects the same small detour in both cases, adding an estimated 2.06 s without changing cumulative ascent. Requirements of 0.1% and 1% fall below the attainable exposure minimum and are infeasible. These results locate the limit of what the model can achieve on the current network; they do not establish that the small feasible reduction has practical value.

Less total climbing also does not mean a gentler route throughout. As reported in Section 4.1, the maximum absolute endpoint grade rises from 0.720807 to 0.769317 on the alternative corridor. This matters when interpreting an ascent preference: a hiker who wants to reduce total climbing may have a different requirement from one who wants to avoid steep sections. The two quantities should therefore remain separate in both the model and the interpretation of its results.

5.2. Implications for route planning

The appropriate formulation depends on the requirement being tested. For a single additive cost, Dijkstra's algorithm and the network LP provide consistent baselines, as their agreement in Section 4.4 confirms. An arc-level grade limit can be handled by filtering the graph before search. Cumulative ascent and exposure budgets require additional resource information. In our formulations, binary variables enforce a single route once these budgets are introduced. The fractional Model 2 solutions in Section 4.2 show why the ordinary LP relaxation is insufficient for those instances.

Combining GPX connections with DEM-derived attributes keeps the route alternatives tied to the recorded trail network while allowing their costs to vary by direction. The same modeling approach could be applied to another area, provided its trail connections and elevation data are checked. Tracing an edge back to a GPX record verifies how it entered the graph, but does not establish that the trail is currently accessible or that its estimated walking time is accurate.

Model 3 is most useful when an additional requirement excludes all fastest routes but leaves a slower alternative available. It can then identify the quickest acceptable route and quantify the time penalty. Proposition 1 describes this case, along with the cases in which the fastest route remains feasible or no route meets the exposure cap. The present OD pairs show only a small opportunity for further exposure reduction, so they provide limited evidence of added practical benefit. For route advice, the limits would also need to reflect independently specified user requirements, and the altitude-weighted exposure index would need an interpretation appropriate to that use.

5.3. Limitations and further Research

The first priority is to test the network and coefficients on which the route choices depend. Coverage is limited to ten GPX tracks, and resampling and spatial merging can affect the available connections. More geographically distinct OD pairs, checked against official trail records, would help determine whether the observed corridor trade-off occurs beyond the two cases studied here. Finer elevation data could improve the representation of steep sections, while sensitivity checks should establish whether the selected routes persist when elevation sampling, node merging, or the speed assumptions change.

Field validation should compare modeled times with recorded journeys and assess whether the exposure measure captures a requirement that users actually want to impose. The present altitude weighting does not measure technical difficulty or cliff exposure. Verified attributes such as trail difficulty, protection, water sources, and shelters could be added where they answer a specific planning question. Independently chosen ascent and exposure limits would also avoid calibrating the requirements around a route that the model has already selected.

Once these inputs are better supported, further extensions could address seasonal closures and uncertain travel times, or present several Pareto-optimal routes with different time, distance, and ascent trade-offs. Robust or stochastic optimization may be useful when uncertainty can be quantified. For the current study, however, testing the stability of the main corridor choice is a more immediate step than adding further objectives or constraints.

6. Conclusion

This study presents a terrain-adapted network-flow framework for optimizing constrained routes on the Brenta Dolomites trail network. The model incorporates distance, ascent, travel time, grade, and altitude-weighted exposure, using Dijkstra's algorithm as a first-stage baseline and MILP as the main optimization tool. The results show that on steep terrain, the best route is not necessarily the shortest one: for Model 2, distance increased by almost 258.15 meters, which brought a reduction in ascent of almost 164.38 meters. Model 3, under the initial constraints, follows the same path as Model 2, and the ablation experiments confirm that this time-optimal route already satisfies the ascent, exposure, and grade constraints on its own, which is why adding them does not change the route.

The main contribution of this study is a practical framework that incorporates terrain characteristics from GPS track data and DEM data, supporting route planning by combining terrain features and user priorities with MILP constraints built on top of the original Dijkstra algorithm. Limitations remain, including data coverage, DEM accuracy, the cost-function assumptions, network granularity, and the choice of internal parameters, but this study lays a foundation for more advanced mountain route planning systems. Future research should draw on more comprehensive terrain and infrastructure data, dynamic conditions, user preferences, and real-world testing to make these models more efficient, accurate, and personalized.

References

[1] Gumus, S., & Turk, Y. (2016). A new skid trail pattern design for farm tractors using linear programing and geographical information systems. *Forests, 7*(12), 306. https://doi.org/10.3390/f7120306

[2] Parsakhoo, A., & Jajouzadeh, M. (2016). Determining an optimal path for forest road construction using Dijkstra's algorithm. *Journal of Forest Science, 62*(6), 264–268. https://doi.org/10.17221/9/2016-JFS

[3] Rees, W. G. (2004). Least-cost paths in mountainous terrain. *Computers & Geosciences, 30*(3), 203–209. https://doi.org/10.1016/j.cageo.2003.11.001

[4] Sferlazza, S., Maltese, A., Ciraolo, G., Dardanelli, G., Maetzke, F. G., & La Mela Veca, D. S. (2021). Forest accessibility, Madonie mountains (northern Sicily, Italy): Implementing a GIS decision support system. *Journal of Maps, 17*(2), 476–485. https://doi.org/10.1080/17445647.2021.1962751

[5] Tobler, W. R. (1993). Three presentations on geographical analysis and modeling: Nonisotropic geographic modeling; speculations on the geometry of geography; and global spatial analysis (Technical Report 93-1). National Center for Geographic Information and Analysis, University of California, Santa Barbara. https://escholarship.org/uc/item/05r820mz

[6] Dijkstra, E. W. (1959). A note on two problems in connexion with graphs. *Numerische Mathematik, 1*, 269–271. https://doi.org/10.1007/BF01386390

[7] Irnich, S., & Desaulniers, G. (2005). Shortest path problems with resource constraints. In G. Desaulniers, J. Desrosiers, & M. M. Solomon (Eds.), *Column generation* (pp. 33–65). Springer. https: //doi.org/10.1007/0-387-25486-2_2

Appendix A. GPX source records

The following URLs are embedded in the archived GPX metadata. They identify the associated route pages, not necessarily the original track authors or the dates on which the project downloaded the files. Eight records point to Outdooractive and two to Trentino.com.

1. Escursione dal Monte Spinale al Passo del Grostè. https://www.trentino.com/it/sport-e-tempo-libero/montagne-ed-escursioni/escursioni-estive/dalmonte-spinale-al-passo-del-groste/
2. Escursione da Pradalago al Lago Gelato. https://www.trentino.com/it/sport-e-tempo-libero/montagne-ed-escursioni/escursioni-alpine/dapradalago-al-lago-gelato/
3. DBT Tappa 4: Rifugio Tuckett - Rifugio ai Brentei https://www.outdooractive.com/r/45969896
4. DBT variante tappa 11: Agritur Malga Tuena - Rifugio Graffer. https://www.outdooractive.com/r/46003797
5. DBT variante tappa 3: Rifugio Graffer - Malga Flavona. https://www.outdooractive.com/r/45921001
6. DBT variante tappa 3: Rifugio Graffer - Malga Spora. https://www.outdooractive.com/r/45921174
7. DBT variante tappa 8: Rifugio Tosa Pedrotti - Rifugio ai Brentei. https://www.outdooractive.com/r/45988269
8. Giro dei rifugi (Rifugio F.F. Tuckett e Q. Sella, Rifugio Casinei). https://www.outdooractive.com/r/50601228
9. Giro dei rifugi (Vallesinella-Casinei-Tuckett-Brentei) https://www.outdooractive.com/r/17631303
10. Giro del Brenta Centrale - Sentiero Orsi https://www.outdooractive.com/r/6117801